SCIENTIFIC REPORTS

OPEN

SUBJECT AREAS:
SYNTHESIS AND PROCESSING
NANOPARTICLES

Received
23 September 2014

Accepted
10 December 2014

Published
19 January 2015

Correspondence and requests for materials should be addressed to H.S.J. (msekorea@kist.re.kr)

A Strategy to enhance Eu^{3+} emission from $LiYF_4$:Eu nanophosphors and green-to-orange multicolor tunable, transparent nanophosphor-polymer composites

Su Yeon Kim[1], Yu-Ho Won[2] & Ho Seong Jang[1]

[1]Center for Materials Architecturing, Korea Institute of Science and Technology, Hwarangno 14-gil 5, Seongbuk-gu, Seoul 136-791, Republic of Korea, [2]Materials Research Center, SAIT, Samsung Electronics Co., 130, Samsung-ro, Youngtong-gu, Suwon-si, Gyeonggi-do 443-803, Republic of Korea.

$LiYF_4$:Eu nanophosphors with a single tetragonal phase are synthesized, and various strategies to enhance the Eu^{3+} emission from the nanophosphors are investigated. The optimized Eu^{3+} concentration is 35 mol%, and the red emission peaks due to the $^5D_0 \rightarrow {}^7F_J$ (J = 1 and 2) transitions of Eu^{3+} ions are further enhanced by energy transfer from a sensitizer pair of Ce^{3+} and Tb^{3+}. The triple doping of Ce, Tb, and Eu into the $LiYF_4$ host more effectively enhances the Eu^{3+} emission than the core/shell strategies of $LiYF_4$:Eu(35%)/$LiYF_4$:Ce(15%), Tb(15%) and $LiYF_4$:Ce(15%), Tb(15%)/$LiYF_4$:Eu(35%) architectures. Efficient energy transfer from Ce^{3+} to Eu^{3+} through Tb^{3+} results in three times higher Eu^{3+} emission intensity from $LiYF_4$:Ce(15%), Tb(15%), Eu(1%) nanophosphors compared with $LiYF_4$:Eu(35%), which contains the optimized Eu^{3+} concentration. Owing to the energy transfer of $Ce^{3+} \rightarrow Tb^{3+}$ and $Ce^{3+} \rightarrow Tb^{3+} \rightarrow Eu^{3+}$, intense green and red emission peaks are observed from $LiYF_4$:Ce(13%), Tb(14%), Eu(1-5%) ($LiYF_4$:Ce, Tb, Eu) nanophosphors, and the intensity ratio of green to red emission is controlled by adjusting the Eu^{3+} concentration. With increasing Eu^{3+} concentration, the $LiYF_4$:Ce, Tb, Eu nanophosphors exhibit multicolor emission from green to orange. In addition, the successful incorporation of $LiYF_4$:Ce, Tb, Eu nanophosphors into polydimethylsiloxane (PDMS) facilitates the preparation of highly transparent nanophosphor-PDMS composites that present excellent multicolor tunability.

Lanthanide ion (Ln^{3+} ion)-doped inorganic crystals have attracted considerable interest due to their unique optical properties, such as high luminescence efficiency and photo- and chemical stability, which facilitated their commercialization in display and illumination devices[1,2]. Among the various Ln^{3+} ions, Eu^{3+} and Tb^{3+} are known to show efficient luminescence and are widely used in such devices[3]. For example, Y_2O_3:Eu^{3+}, (Y,Gd)BO_3:Eu^{3+}, Y_2O_2S:Eu^{3+} have been used in fluorescent lamps (FLs), plasma display panels (PDPs), cathode ray tubes (CRTs), respectively[2,4]. In the case of Tb^{3+} ions, $LaPO_4$:Ce^{3+}, Tb^{3+}, Gd_2O_2S:Tb^{3+}, and YBO_3:Tb^{3+} have been used in FLs, scintillators, and PDPs, respectively[2,5]. Thus, many studies have been published on Eu^{3+}- and Tb^{3+}-activated inorganic crystals, which are known as phosphors[2–6]. In 1999, Meijerink and colleagues introduced efficient red-emitting $LiGdF_4$:Eu^{3+} phosphors that demonstrated a quantum efficiency (QE) greater than 100% via the quantum cutting (QC) process[7]. Such QC phosphors can be applied to solar cells for the improvement of solar cell efficiency by converting ultraviolet (UV) light into visible light with increased photon numbers[8,9]. However, for application in solar cells, nanometer-sized QC phosphors (i.e., QC nanophosphors) should be used to minimize incident light scattering because the QC phosphors are located in front of the Si solar cell[8,10]. Recently, thanks to the development of synthetic methodology, well-defined nanophosphors of uniform size were successfully synthesized via thermal decomposition, hydrothermal, and co-precipitation methods, among others[11–21]. However, to the best of our knowledge, there have been no reports on $LiGdF_4$:Eu^{3+} nanophosphors. This may be partly attributed to the difficulty associated with the synthesis of single-tetragonal-phase $LiGdF_4$ nanocrystals (NCs)[22,23]. On the other hand, $LiYF_4$, which has the same crystal structure as $LiGdF_4$, can also be

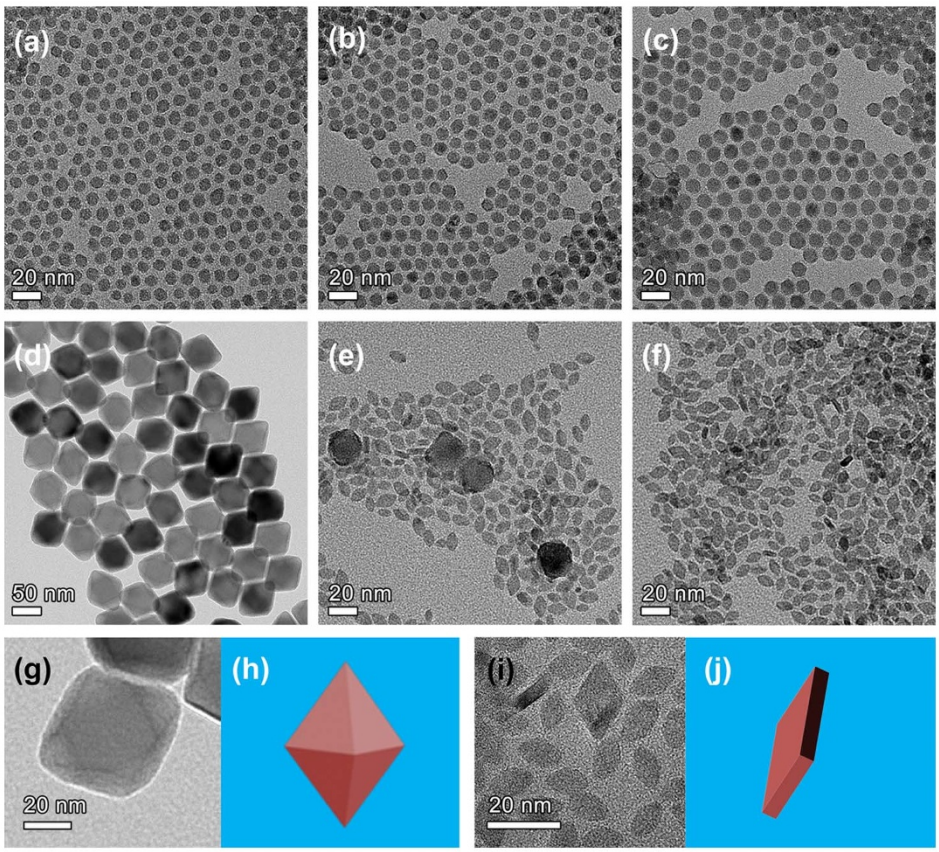

Figure 1 | TEM images of $LiYF_4$:Eu nanophosphors with varying Eu^{3+} concentrations of (a) 10%, (b) 20%, (c) 30%, (d) 35%, (e) 40%, (f) 45%, and (g and i) high magnification TEM images of $LiYF_4$:Eu(35%) and $LiYF_4$:Eu(45%), and (h and j) corresponding schematic morphologies for $LiYF_4$:Eu(35%) and $LiYF_4$:Eu(45%), respectively.

considered as a host crystal for nanophosphors[24–26]. Because of its inherently low lattice phonon energy, $LiYF_4$ has been used as a host crystal for upconversion phosphors[24–26]. Similar to the cases of $NaYF_4$ and $NaGdF_4$ as host materials[27,28], $LiYF_4$ may be a good candidate for downshifting phosphors as well as a promising host lattice for upconversion[29,30]. In this article, we report on the luminescence properties of $LiYF_4$:Eu^{3+} ($LiYF_4$:Eu) colloidal nanophosphors. To the best of our knowledge, colloidal $LiYF_4$:Eu nanophosphors have not yet been reported although micrometer-sized (larger than 10 μm) $LiYF_4$:Eu particles have been reported[31]. To enhance the emission intensity of $LiYF_4$:Eu and achieve multicolor emission, Tb^{3+} was employed as a sensitizer. Multicolor emission is another advantage of Ln^{3+} ion-doped nanophosphors[32,33]. Tunable multicolor emission coupled with size- and shape-independent luminescence under single wavelength excitation is beneficial for multicolor labeling and display device applications[16,32]. Energy transfer from a sensitizer ion to the Eu^{3+} ion is a favorable solution for achieving enhanced Eu^{3+} emission[6] and multicolor luminescence[16,34]. To obtain efficient energy transfer from the Tb^{3+} sensitizer to the Eu^{3+} ion, we used various approaches. First, we synthesized nanophosphors with a core/shell architecture in which Eu^{3+} and Tb^{3+} ions were separately doped within the core and the shell. We also synthesized Eu^{3+} and Tb^{3+} co-doped single-$LiYF_4$ NCs. In addition, Ce^{3+} ions were used as sensitizers for enhanced luminescence and single wavelength excitation because the 4f-5d electronic transition in a Ce^{3+} ion is a spin- and parity-allowed transition and the Ce^{3+} ion has a large absorption cross-section[16,35]. That is, $LiYF_4$:Eu/$LiYF_4$:Ce^{3+}, Tb^{3+} ($LiYF_4$:Ce, Tb), $LiYF_4$:Ce, Tb/$LiYF_4$:Eu, and $LiYF_4$:Ce^{3+}, Tb^{3+}, Eu^{3+} ($LiYF_4$:Ce, Tb, Eu) nanophosphors were synthesized, and their luminescence properties were investigated. Furthermore, multicolor emission from green to orange was successfully realized by varying the Tb^{3+} and Eu^{3+} concentrations, and the feasibility of their use in a transparent display application was examined through the fabrication of multicolor-emitting polymer composites.

Results

$LiYF_4$:Eu nanophosphors with various Eu^{3+} concentrations were synthesized to achieve strong red luminescence. Figure 1 shows transmission electron microscopy (TEM) images of the $LiYF_4$:Eu nanophosphors. Until 35 mol% Eu^{3+} doping, the $LiYF_4$:Eu nanophosphors showed uniform size and shape (Figures 1a–d). However, when the concentration of Eu^{3+} was 40 mol%, both large and small particles were simultaneously observed (Figure 1e). When the concentration of Eu^{3+} was greater than 40 mol%, uniform small particles were obtained (Figure 1f). This morphological change was attributed to the crystal structure of the $LiYF_4$:Eu. For Eu^{3+} concentrations less than 40 mol%, nanocrystals (NCs) with a single tetragonal phase were synthesized (see X-ray diffraction (XRD) patterns of Figure S1). When 40 mol% of Eu^{3+} dopant was incorporated, mixed phases of tetragonal and orthorhombic structures were synthesized, whereas NCs with an orthorhombic structure was formed with Eu^{3+} concentrations greater than 40 mol%. As shown in Figure 1, the particle size increased slightly from 8.0 ± 0.7 to 10.0 ± 0.6 nm as the doping concentration of Eu^{3+} ions was increased to 30 mol%. Then, large tetragonal bipyramidal particles with edge lengths of 63.2 ± 2.2 nm × 68.4 ± 1.9 nm were synthesized under a Eu^{3+} doping condition of 35 mol%. This result is similar to finding in our previously reported work[23]. Doping the Y^{3+} sites with ions that are larger than the Y^{3+} ion induces the large particle size due to the presence of less negatively charged F^- ions at the (101) surface layer of the $LiYF_4$ crystals[23]. However, too much Eu^{3+} doping led to the

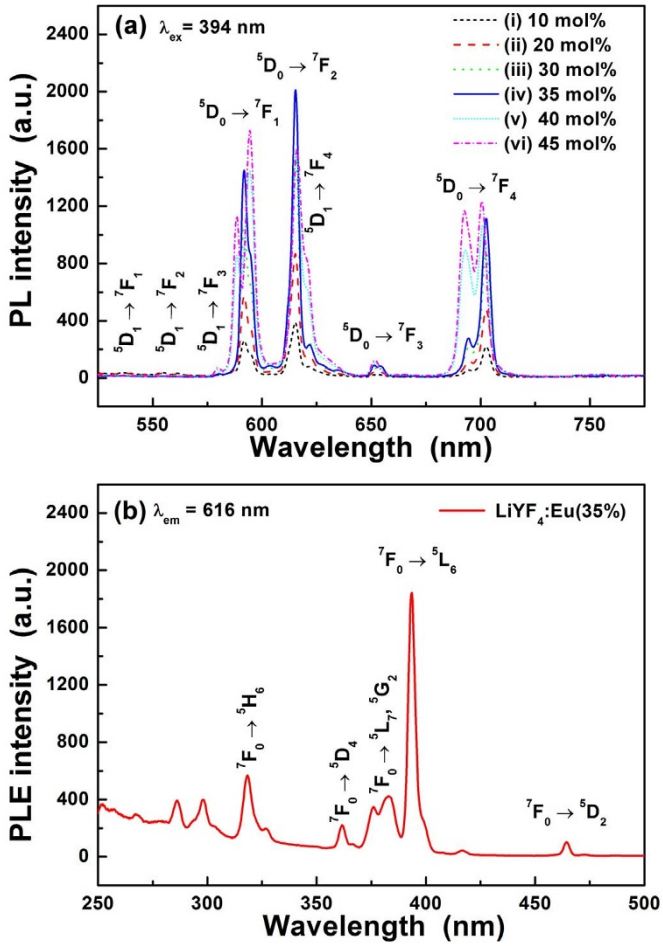

Figure 2 | (a) PL spectra of $LiYF_4$:Eu(10–45%) nanophosphors under the excitation of 394 nm and (b) PLE spectrum of $LiYF_4$:Eu(35%) nanophosphors monitored at 616 nm [(i) 10%, (ii) 20%, (iii) 30%, (iv) 35%, (v) 40%, and (vi) 45%].

formation of orthorhombic YF_3 NCs. According to Du et al. and Ye et al., the orthorhombic phase, instead of the tetragonal phase, readily forms under large Eu^{3+} fraction[22,36]. Due to different crystal structures, $LiYF_4$:Eu exhibited a tetragonal bipyramidal morphology, as shown in Figures 1g and h (see also scanning transmission electron microscopy (STEM) image of $LiYF_4$:Eu(35%) in Figure S2), and YF_3:Eu showed a rhombic plate shape, as shown in Figures 1i and j.

Figure 2 shows photoluminescence (PL) and photoluminescence excitation (PLE) spectra of $LiYF_4$:Eu nanophosphors. Sharp emission peaks can be observed in the red spectral region of the PL spectra. These peaks were attributed to the electronic transitions from the excited $^5D_1$ and $^5D_0$ levels to the ^7F_J (J = 0–6) levels[3]. As shown in Figure 2a, a strong emission peak at approxmately 610–620 nm can be ascribed to the hypersensitive electric dipole transition of the $^5D_0 \rightarrow {}^7F_2$ transition. The emission peak at approximately 590–600 nm is due to the magnetic dipole transition of $^5D_0 \rightarrow {}^5F_1$, which is lower than that due to the $^5D_0 \rightarrow {}^7F_2$ transition, indicating that Eu^{3+} ions are located at the non-inversion symmetric sites[6,37]. As the Eu^{3+} concentration was increased to 35 mol% in the $LiYF_4$ host crystals, the PL intensity increased as well. At higher Eu^{3+} concentrations, the PL intensity decreased. In addition, when the Eu^{3+} concentration was 45 mol%, the shape of the PL spectrum differed from that of the $LiYF_4$:Eu(35%) nanophosphors. In this case, a single orthorhombic structure was formed, and the PL intensity due to the $^5D_0 \rightarrow {}^7F_1$ transition was higher than that due to the $^5D_0 \rightarrow {}^7F_2$ transition.

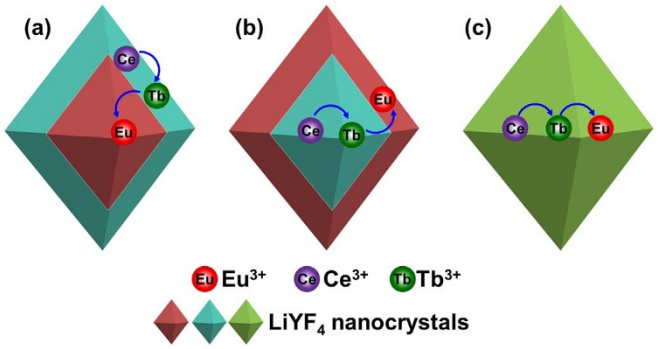

Figure 3 | Schematic illustrations showing various architectures for enhancement of Eu^{3+} emission from $LiYF_4$:Eu-based nanophosphors (a) $LiYF_4$:Eu/$LiYF_4$:Ce, Tb core/shell, (b) $LiYF_4$:Ce, Tb/$LiYF_4$:Eu core/shell, and (c) $LiYF_4$:Ce, Tb, Eu nanophosphors.

The strongest PLE peak can be observed at 394 nm (Figure 2b). This peak was attributed to the $^7F_0 \rightarrow {}^5L_6$ transition. Because the charge transfer band of Eu^{3+}-F^- lies within the vacuum ultraviolet (VUV) region (approximately 150 nm)[7], a broad PLE band due to charge transfer was not observed (Figure 2b). Upon considering the first spin allowed f–d transition, the 4f–5d transition band is also found to lie within the VUV region (approximately 143 nm). According to Dorenbos[38], the f–d energy difference of Eu^{3+} ions doped in $LiYF_4$, $E(Eu, LiYF_4)$ can be expressed as follows:

$$E(Eu,LiYF_4) = 49{,}340\ cm^{-1} - D(Ce,LiYF_4) + \Delta E^{Eu,Ce} \qquad (1)$$

where 49,340 cm^{-1} is the energy of the first f–d transition of Ce^{3+} as a free ion, D(Ce, $LiYF_4$) is the crystal field depression, which is defined as the lowering of this energy when the Ce^{3+} ion is doped in $LiYF_4$, and $\Delta E^{Eu,Ce}$ is defined as the difference in the f–d energy of Eu^{3+} relative to that of the first electric dipole allowed transition in Ce^{3+}[38]. Taking D(Ce, $LiYF_4$) = 15,262 cm^{-1} and $\Delta E^{Eu,Ce}$ = 35,900 ± 380 cm^{-1} for $LiYF_4$, the f–d transition band of Eu^{3+} ions in the $LiYF_4$ host crystal is expected to reside at 69,978 ± 380 cm^{-1} (approximately 143 nm)[38]. Thus, broad excitation bands due to either charge transfer or the 4f–5d transition were not observed in the UV spectral region, whereas sharp excitation peaks due to the f-f transition can be observed in Figure 2b. In this spectral range, concentration of the activator Eu^{3+} ions was linearly related to the PL intensity, indicating that Eu^{3+} emission results from the direct excitation-emission of Eu^{3+} ions[39].

As shown in Figures 1 and 2, the optimized Eu^{3+} concentration in terms of the PL intensity was 35 mol%, and further increasing the Eu^{3+} doping fraction induced a phase transformation from tetragonal $LiYF_4$ to the orthorhombic YF_3 phase. To further enhance the Eu^{3+} emission in $LiYF_4$ NCs, other strategies besides increasing the Eu^{3+} concentration are needed. Energy transfer from a sensitizer to the Eu^{3+} ions can be a good pathway for enhancing Eu^{3+} luminescence. Previously, Wang et al. reported that Ce^{3+} ions can be a sensitizer for Eu^{3+} emission[35]. However, as shown in Figure S3, when Ce^{3+} and Eu^{3+} were co-doped in $LiYF_4$ NCs, orthorhombic phase YF_3 impurities were formed at a low Eu^{3+} concentration of 15 mol% compared with $LiYF_4$:Eu^{3+} nanophosphors. In addition, the $^5D_0 \rightarrow {}^7F_2$ emission was stronger under Eu^{3+} direct excitation at 394 nm than under the $Ce^{3+} \rightarrow Eu^{3+}$ energy transfer condition excited at 300 nm (Figure S3f). These results indicate that the use of Ce^{3+} sensitization alone is incapable of significantly enhancing Eu^{3+} emission in the $LiYF_4$ NCs. Recently, we reported on the high efficiency of the $Ce^{3+} \rightarrow Tb^{3+} \rightarrow Eu^{3+}$ energy transfer pathway[16]. Thus, we adopted Ce^{3+} and Tb^{3+} ions as co-sensitizers and synthesized various structures of $LiYF_4$:Eu-based nanophosphors, as shown

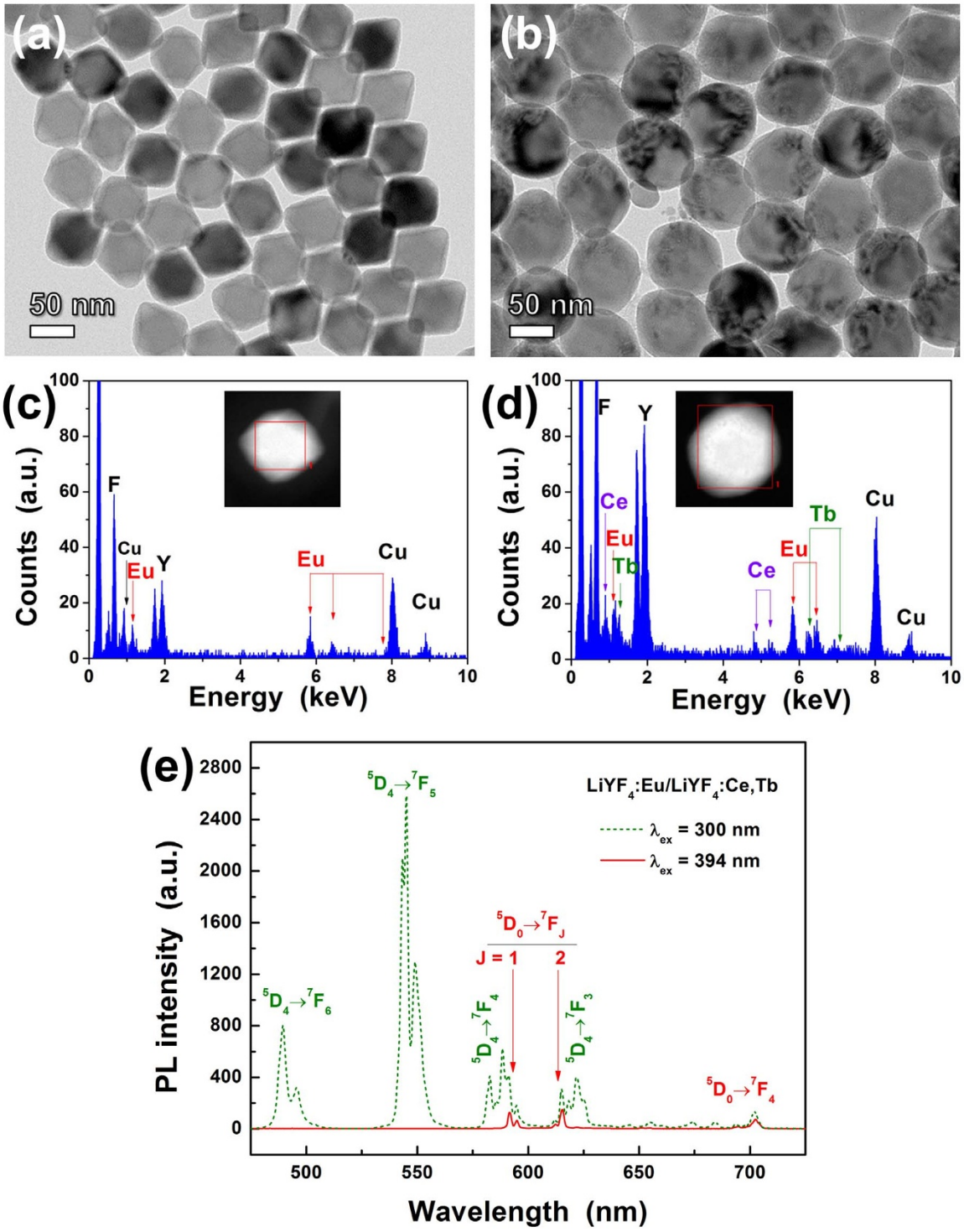

Figure 4 | (a), (b) TEM images, (c), (d) EDS spectra of $LiYF_4$:Eu(35%) and $LiYF_4$:Eu(35%)/$LiYF_4$:Ce(15%), Tb(15%) nanophosphors, respectively, and (e) PL spectra of $LiYF_4$:Eu(35%)/$LiYF_4$:Ce(15%), Tb(15%) nanophosphors under the excitations of 300 nm (dotted green line) and 394 nm (solid red line). Insets of (c) and (d) show STEM images of a single $LiYF_4$:Eu(35%) and $LiYF_4$:Eu(35%)/$LiYF_4$:Ce(15%), Tb(15%) nanophosphors, where EDS spectra were obtained for red squares, respectively.

in Figure 3. Then, we investigated the various nanophosphor architectures for strong Eu^{3+} emission. Figures 3a and b show schematic illustrations of $LiYF_4$:Eu/$LiYF_4$:Ce, Tb and $LiYF_4$:Ce, Tb/$LiYF_4$:Eu core/shell nanophosphors. Ghosh et al. reported enhanced Tb^{3+} emission via energy transfer from Ce^{3+} ions (sensitizer) in the $NaYF_4$ core to Tb^{3+} ions in the $NaYF_4$ shell[40]. On the other hand, Capobianco's group reported enhanced Er^{3+} emission via the additional energy transfer from Yb^{3+} ions in the $NaGdF_4$ shell to Er^{3+} ions in the $NaGdF_4$ core[41]. In these core/shell structured nanophosphors, optimized Eu^{3+} concentrations can be doped into $LiYF_4$ NCs because Eu^{3+} ions are singly doped into either the $LiYF_4$ core or the $LiYF_4$ shell. Figure 3c shows a schematic illustration of Ce^{3+}, Tb^{3+}, and Eu^{3+} triply-doped $LiYF_4$ nanocrystals. Next, the aforementioned three types of nanophosphors were synthesized, and their luminescence properties were investigated.

Figures 4a and b show TEM images of $LiYF_4$:Eu(35%) core and $LiYF_4$:Eu(35%)/$LiYF_4$:Ce(15%), Tb(15%) core/shell nanophosphors.

The particle size increased after shell formation on the $LiYF_4$:Eu(35%) cores. Energy dispersive X-ray spectroscopy (EDS) analyses indicated that core/shell structured nanophosphors were successfully synthesized (Figures 4c and d). In the EDS spectrum of a single $LiYF_4$:Eu(35%)/$LiYF_4$:Ce(15%), Tb(15%) nanoparticle, Ce and Tb peaks as well as Eu peaks were observed, whereas only Eu peaks were observed in the EDS spectrum of a single $LiYF_4$:Eu(35%) core nanoparticle. Combining the XRD patterns (Figure S4) with EDS spectra (Figures 4 and S5) confirmed that $LiYF_4$:Eu(35%)/$LiYF_4$:Ce(15%), Tb(15%) core/shell nanophosphors with a single tetragonal phase were synthesized. As shown in Figure 4e, Eu^{3+} emission was enhanced via the $Ce^{3+} \rightarrow Tb^{3+} \rightarrow Eu^{3+}$ energy transfer pathway. The PL intensity of Eu^{3+} emission from the $LiYF_4$:Eu(35%)/$LiYF_4$:Ce(15%), Tb(15%) core/shell nanophosphors under excitation with 300 nm UV light was higher than that under excitation with 394 nm light, which directly excited the Eu^{3+} ions. From the PLE spectrum in Figure S6, we can directly compare the Eu^{3+} emission intensity due to the $^7F_0 \rightarrow {}^5L_6$ transition of Eu^{3+} with that due to the 4f → 5d transition of Ce^{3+}. As a result, it was found that the $Ce^{3+} \rightarrow Tb^{3+} \rightarrow Eu^{3+}$ energy transfer is more effective for intense Eu^{3+} emission than Eu^{3+} direct excitation-emission because the PLE intensity due to the 4f → 5d band excitation of Ce^{3+} was higher than that due to the $^7F_0 \rightarrow {}^5L_6$ excitation of Eu^{3+}. It should be noted that a fraction of the excited energy can be directly transferred from Ce^{3+} to Eu^{3+}, as shown in Figure S3f. In addition to Eu^{3+} emission peaks, Tb^{3+} characteristic emission peaks were observed via the $^5D_4 \rightarrow {}^7F_J$ (J = 6, 5, 4, and 3) through $Ce^{3+} \rightarrow Tb^{3+}$ energy transfer (Figure 4e).

The luminescence properties of the $LiYF_4$:Ce(15%), Tb(15%)/$LiYF_4$:Eu(35%) core/shell nanophosphors were also investigated. Figures 5a and b show TEM images of $LiYF_4$:Ce(15%), Tb(15%) core nanophosphors and $LiYF_4$:Ce(15%), Tb(15%)/$LiYF_4$:Eu(35%) core/shell nanophosphors. The particle size increased from 31.6 ± 1.0 nm × 32.7 ± 1.1 nm to 37.7 ± 1.4 nm × 39.3 ± 1.5 nm after $LiYF_4$:Eu shell formation on the $LiYF_4$:Ce, Tb core, and only $LiYF_4$:Ce(15%), Tb(15%)/$LiYF_4$:Eu(35%) exhibited Eu peaks in the EDS spectra, as shown in Figures 5c and d. A single tetragonal phase was observed in both the $LiYF_4$:Ce(15%), Tb(15%)/$LiYF_4$:Eu(35%) nanophosphors and $LiYF_4$:Ce(15%), Tb(15%) nanophosphors (Figure S7). Figure S8 shows EDS spectra obtained at different locations (center and edge) of individual $LiYF_4$:Ce(15%), Tb(15%) core and $LiYF_4$:Ce(15%), Tb(15%)/$LiYF_4$:Eu(35%) core/shell nanoparticles. In the EDS spectra of core nanoparticles, peaks associated with Ce and Tb were observed, whereas Eu peaks were not observed at either central or edge regions of the core nanoparticles (Figures S8a and b). In the core/shell nanoparticles, the intensity of the Eu peak was strong, whereas the Ce and Tb peaks were very weak at the edge region. By contrast, the intensities of the Ce and Tb peaks were strong and that of the Eu peak was very weak at the central region of the $LiYF_4$:Ce(15%), Tb(15%)/$LiYF_4$:Eu(35%) core/shell nanoparticle (Figures S8c and d). These TEM, XRD, and EDS results support that $LiYF_4$:Ce(15%), Tb(15%)/$LiYF_4$:Eu(35%) nanophosphors were successfully synthesized with a single tetragonal structure. Figure 5e shows the PL spectra of $LiYF_4$:Ce(15%), Tb(15%)/$LiYF_4$:Eu(35%) nanophosphors excited at 300 and 394 nm. Like the case of $LiYF_4$:Eu(35%)/$LiYF_4$:Ce(15%), Tb(15%) excited at 300 nm, Tb^{3+} characteristic emission peaks via $Ce^{3+} \rightarrow Tb^{3+}$ energy transfer were observed together with Eu^{3+} emission peaks under excitation with 300 nm UV light. However, the PL intensity due to the $^5D_0 \rightarrow {}^7F_2$ transition of the Eu^{3+} ions was lower under excitation with 300 nm light compared with excitation with 394 nm light. This finding indicates that Eu^{3+} emission is more efficient for the direct excitation of Eu^{3+} than for the indirect Eu^{3+} excitation via energy transfer of $Ce^{3+} \rightarrow (Tb^{3+}) \rightarrow Eu^{3+}$ in the $LiYF_4$:Ce(15%), Tb(15%)/$LiYF_4$:Eu(35%) nanophosphors. As shown in Figure 2b, a weak PLE peak can be observed in the UV spectral region (approximately 300 nm), and thus some fraction of externally originating UV light can be absorbed by the $LiYF_4$:Eu shell before absorption by Ce^{3+} in the core. Therefore, external UV light was not fully absorbed by Ce^{3+} ions in the $LiYF_4$:Ce, Tb core, and less excited energy was transferred from Ce^{3+} to Eu^{3+} through Tb^{3+} compared with the case of $LiYF_4$:Eu(35%)/$LiYF_4$:Ce(15%), Tb(15%) core/shell nanophosphors.

In addition to core/shell structured nanophosphors, the luminescence properties of Ce^{3+}, Tb^{3+}, and Eu^{3+} triply-doped $LiYF_4$ NCs are shown in Figure 6. The $LiYF_4$:Ce, Tb, Eu nanophosphors can also be synthesized with a core/shell sturcture, and Figures 6a and b show TEM images of $LiYF_4$:Ce(15%), Tb(15%), Eu(1%) and $LiYF_4$:Ce(15%), Tb(15%), Eu(1%)/$LiYF_4$ nanophosphors. When the Eu^{3+} concentration was larger than 1%, a single tetragonal bipyramidal shape did not form; instead mixed morphologies of tetragonal bipyramids and rhombic plates were observed in TEM image (Figure S9a). Although the Eu^{3+} concentration of $LiYF_4$:Ce(15%), Tb(15%), Eu(1%) nanophosphors was significantly smaller than that of $LiYF_4$:Eu(35%), the $LiYF_4$:Ce(15%), Tb(15%), Eu(1%) nanophosphors showed much stronger Eu^{3+} emission intensities under excitation with 300 nm light, which excited the Ce^{3+} ions. As shown in Figure 6c, the Eu^{3+} emission intensity of the $LiYF_4$:Ce(15%), Tb(15%), Eu(1%) under excitation with 300 nm light was three times higher than that of $LiYF_4$:Eu(35%) under excitation with 394 nm light. This result means that the $Ce^{3+} \rightarrow Tb^{3+} \rightarrow Eu^{3+}$ energy transfer is very efficient in the Ce^{3+}, Tb^{3+}, and Eu^{3+} triply-doped $LiYF_4$ nanophosphors. In conclusion, in the case of $LiYF_4$ host crystals, the Ce^{3+}, Tb^{3+}, and Eu^{3+} triply-doped system was the most efficient for obtaining strong Eu^{3+} emission compared with the core/shell structured nanophosphors shown in Figure 3. Furthermore, the emission intensity of the nanophosphor was further enhanced by growing a $LiYF_4$ shell on the $LiYF_4$:Ce(15%), Tb(15%), Eu(1%) core. After forming the $LiYF_4$ shell on the core, the particle size was slightly increased (Figure 6b), and EDS spectra obtained from individual particles confirmed the formation of a core/shell structure (Figure S10). Thanks to the formation of a $LiYF_4$ shell on the core, the PL intensity of the $LiYF_4$:Ce(15%), Tb(15%), Eu(1%)/$LiYF_4$ core/shell nanophosphors was 62% higher than that of the core nanophosphors. As a result, the Eu^{3+} emission intensity of the core/shell nanophosphors was 4.6 times greater than that of the $LiYF_4$:Eu(35%) nanophosphors (Figure 6c). In the Ce, Tb, and Eu triply-doped phosphor system, it was reported that Tb blocks the Ce-Eu charge transfer[42,43]. However, weak Ce^{4+}-related peaks were observed with strong Ce^{3+}-related peaks in the X-ray photoelectron spectroscopy (XPS) spectrum of $LiYF_4$:Ce(15%), Tb(15%), Eu(1%) (Figure S11). In particular, the specific peak at 917 eV, which is frequently taken as confirmation of the presence of Ce^{4+}, was observed in the XPS spectrum[44,45]. Although Ce^{4+}-related peaks were very weak and negligible, there might be probability of the exsitence of the electron transfer relation ($Ce^{3+} + Eu^{3+} \rightarrow Ce^{4+} + Eu^{2+}$).

Multicolor emission from the $LiYF_4$:Ce, Tb, Eu nanophosphors was realized by varying the ratio of the Tb^{3+} to Eu^{3+} emission intensities. The desired outcome was readily achieved by adjusting the Eu^{3+} concentrations. However, as shown in Figure S9, when the Eu^{3+} concentration was 2 mol%, an impurity YF_3 phase was synthesized. According to Du et al., light lanthanide ions in the Y^{3+} sites of $LiYF_4$ resists the formation of a single tetragonal phase[22]. Thus, to increase the Eu^{3+} quantities in the $LiYF_4$ host, the amounts of Ce^{3+} and Tb^{3+} were reduced. Figure S12 shows XRD patterns of $LiYF_4$:Ce(13%), Tb(14%), Eu(1–5%) ($LiYF_4$:Ce, Tb, Eu) nanophosphors. These XRD patterns confirmed that all of the synthesized nanophosphors had a single tetragonal phase. Figure 7 shows PL and PLE spectra, and the Commission Internationale de l'Eclairage (CIE) color coordinates of the $LiYF_4$:Ce, Tb, Eu nanophosphors with varying Eu^{3+} concentrations. As the Eu^{3+} concentration increased, the intensity ratio of the Tb^{3+} emission to the Eu^{3+} emission decreased (Figures 7a and S13). Although the Ce^{3+} and Tb^{3+} concentrations decreased

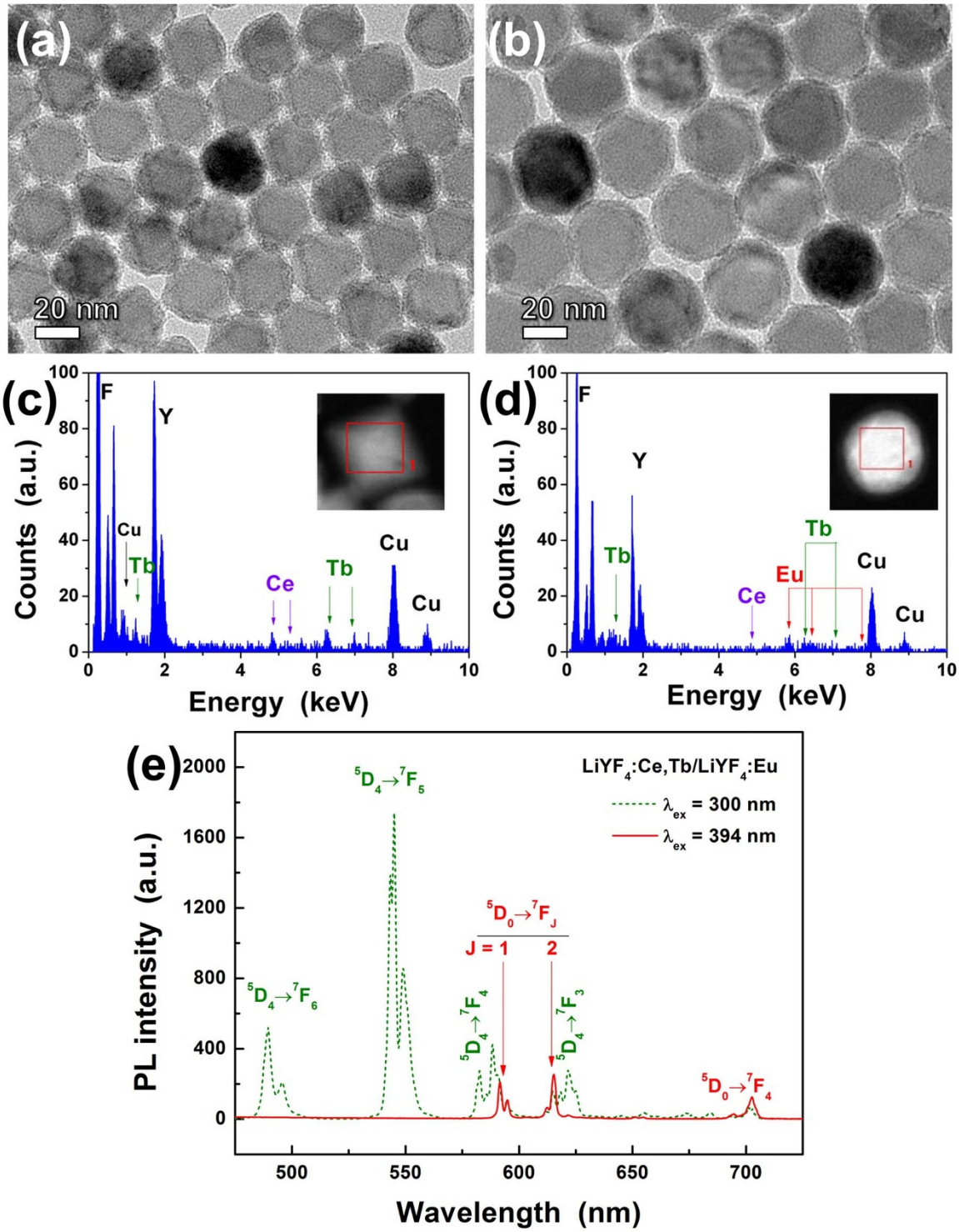

Figure 5 | (a), (b) TEM images, (c), (d) EDS spectra of $LiYF_4$:Ce(15%), Tb(15%) and $LiYF_4$:Ce(15%), Tb(15%)/$LiYF_4$:Eu(35%) nanophosphors, respectively, and (e) PL spectra of $LiYF_4$:Ce(15%), Tb(15%)/$LiYF_4$:Eu(35%) nanophosphors under the excitations of 300 nm (dotted green line) and 394 nm (solid red line). Insets of (c) and (d) show STEM images of a single $LiYF_4$:Ce(15%), Tb(15%) and $LiYF_4$:Ce(15%), Tb(15%)/$LiYF_4$:Eu(35%) nanophosphor, where EDS spectra were obtained for red squares, respectively.

slightly compared with $LiYF_4$:Ce(15%), Tb(15%), Eu(1%), the Eu^{3+} emission remained strong under excitation with 300 nm light. The Eu^{3+} emission intensity of $LiYF_4$:Ce(13%), Tb(14%), Eu(3%) under excitation with 300 nm light was 3.1 times greater than that of $LiYF_4$:Eu(35%) under excitation with 394 nm light (Figure 7b). As shown in the PLE spectra of Figure 7c, strong broad bands were observed in the UV region due to the 4f → 5d transition of Ce^{3+} ions, indicating the energy transfer from Ce^{3+} to Eu^{3+}. According to Zhang et al. and Blasse, Tb^{3+} acts as an energy transfer mediator, bridging the energy transfer from Ce^{3+} to Eu^{3+} and blocks the corresponding metal-metal charge transfer[42,43]. When we compared the Eu^{3+} emission intensity of $LiYF_4$:Ce(13%), Tb(14%), Eu(1%) with that of $LiYF_4$:Ce(13%), Eu(1%), the $LiYF_4$:Ce(13%), Tb(14%), Eu(1%) exhibited the significantly higher PL intensity (Figure S14).

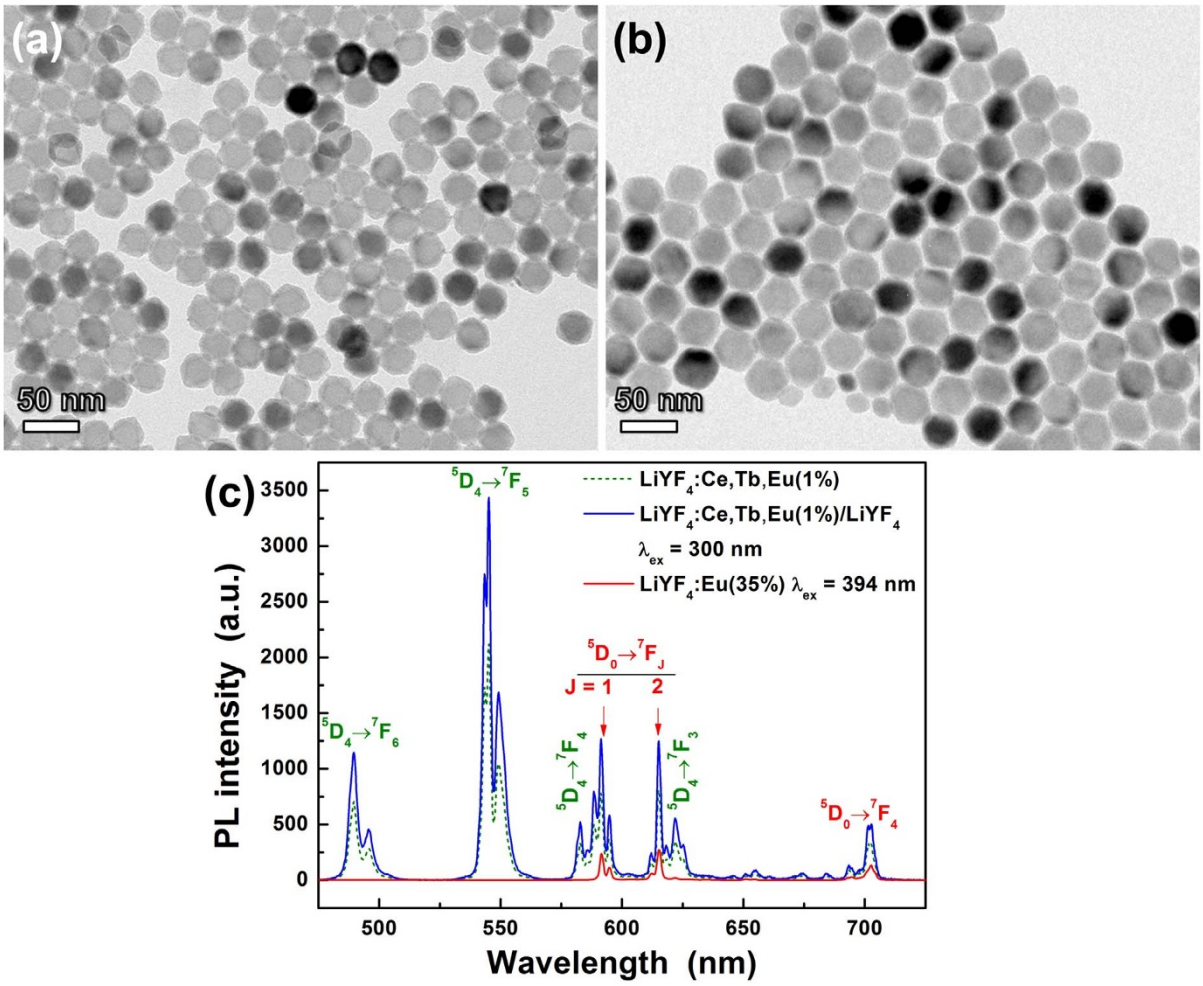

Figure 6 | (a), (b) TEM images of $LiYF_4$:Ce(15%), Tb(15%), Eu(1%) and $LiYF_4$:Ce(15%), Tb(15%), Eu(1%)/$LiYF_4$ and (c) PL spectra of $LiYF_4$:Ce(15%), Tb(15%), Eu(1%) (dotted green line) and $LiYF_4$:Ce(15%), Tb(15%), Eu(1%)/$LiYF_4$ (solid blue line) under the excitation of 300 nm, and $LiYF_4$:Eu(35%) (solid red line) under the excitation of 394 nm.

This result confirms that the $Ce^{3+} \rightarrow Tb^{3+} \rightarrow Eu^{3+}$ energy transfer is more efficient than $Ce^{3+} \rightarrow Eu^{3+}$ energy transfer. The $LiYF_4$:Ce(13%), Tb(14%), Eu(1%) nanophosphors emitted yellow-green light due to the intense $^5D_4 \rightarrow {}^7F_5$ transition of Tb^{3+} and weak $^5D_0 \rightarrow {}^7F_2$ transition of Eu^{3+} under excitation at 300 nm. The ratio of the PL intensity in the green spectral region due to the $^5D_4 \rightarrow {}^7F_5$ transition of Tb^{3+} ions to that in the red spectral region due to the $^5D_0 \rightarrow {}^7F_2$ transition of Eu^{3+} ions decreased with increasing Eu^{3+} concentration (Figure S13). As a result, the emission color of the $LiYF_4$:Ce, Tb, Eu nanophosphors gradually transitioned from green to orange as a function of the Eu^{3+} concentration. The CIE color coordinates (x, y) of the $LiYF_4$:Ce, Tb, Eu nanophosphors shifted from (0.3484, 0.5799) to (0.4936, 0.4675), as shown in Figure 7d. The gradual luminescence color shift from green to orange was directly confirmed with imaging showing the luminescence of $LiYF_4$:Ce, Tb, Eu solutions illuminated with a hand-held UV lamp (Figure 7d inset).

Discussion

In the PLE spectra of Figure 7c, the PLE band due to the 4f → 5d transition of Ce^{3+} ions was strong, whereas the PLE peak of the $^7F_6 \rightarrow {}^5D_4$ transition of Tb^{3+} ions at 487 nm was very weak (almost negligible). The weak PLE peak at 487 nm can be attributed to the weak excitation of Tb^{3+} ions at this wavelength and/or inefficient energy transfer from the Tb^{3+} to Eu^{3+} ions. When the PLE spectra of $LiYF_4$:Ce, Tb, Eu(1–5%) were monitored at 545 nm for Tb^{3+} emission, the PLE peaks were also very weak at 487 nm, which is the direct excitation wavelength of Tb^{3+} (Figure S15). This result indicates that the weak PLE peak at 487 nm in Figure 7c was attributed to the weak direct excitation of Tb^{3+} at this wavelength. Thus, to confirm the energy transfer from Tb^{3+} to Eu^{3+}, the decay time for Tb^{3+} emission was examined, although the $LiYF_4$:Ce, Tb, Eu showed much stronger Eu^{3+} emission than $LiYF_4$:Ce, Eu. According to Dexter theory[46], the probability of energy transfer via multipolar interaction can be expressed by the following equation

$$P(R) \propto \frac{Q_A}{R^b \tau_D} \int \frac{f_D(E) F_A(E)}{E^c} dE \qquad (2)$$

where P is the energy transfer probability, τ_D is the decay time of the donor emission, Q_A is the total absorption cross-section of the acceptor, R is the distance between the donor and the acceptor, and b and c are parameters that depend on the type of energy transfer. Figure 8a shows the decay profiles of $LiYF_4$:Ce, Tb, Eu nanophosphors monitored at 545 nm for Tb^{3+} emission with varying Eu^{3+} concentrations. The decay time of the Tb^{3+} emission was observed to shorten with increasing Eu^{3+} concentration. According to equation (2), because the energy transfer probability P is inversely proportional to the decay time of τ_D, the shortened decay time of the Tb^{3+} emission confirms the presence of an energy transfer pathway from Tb^{3+} to Eu^{3+}. To better understand the process of energy trans-

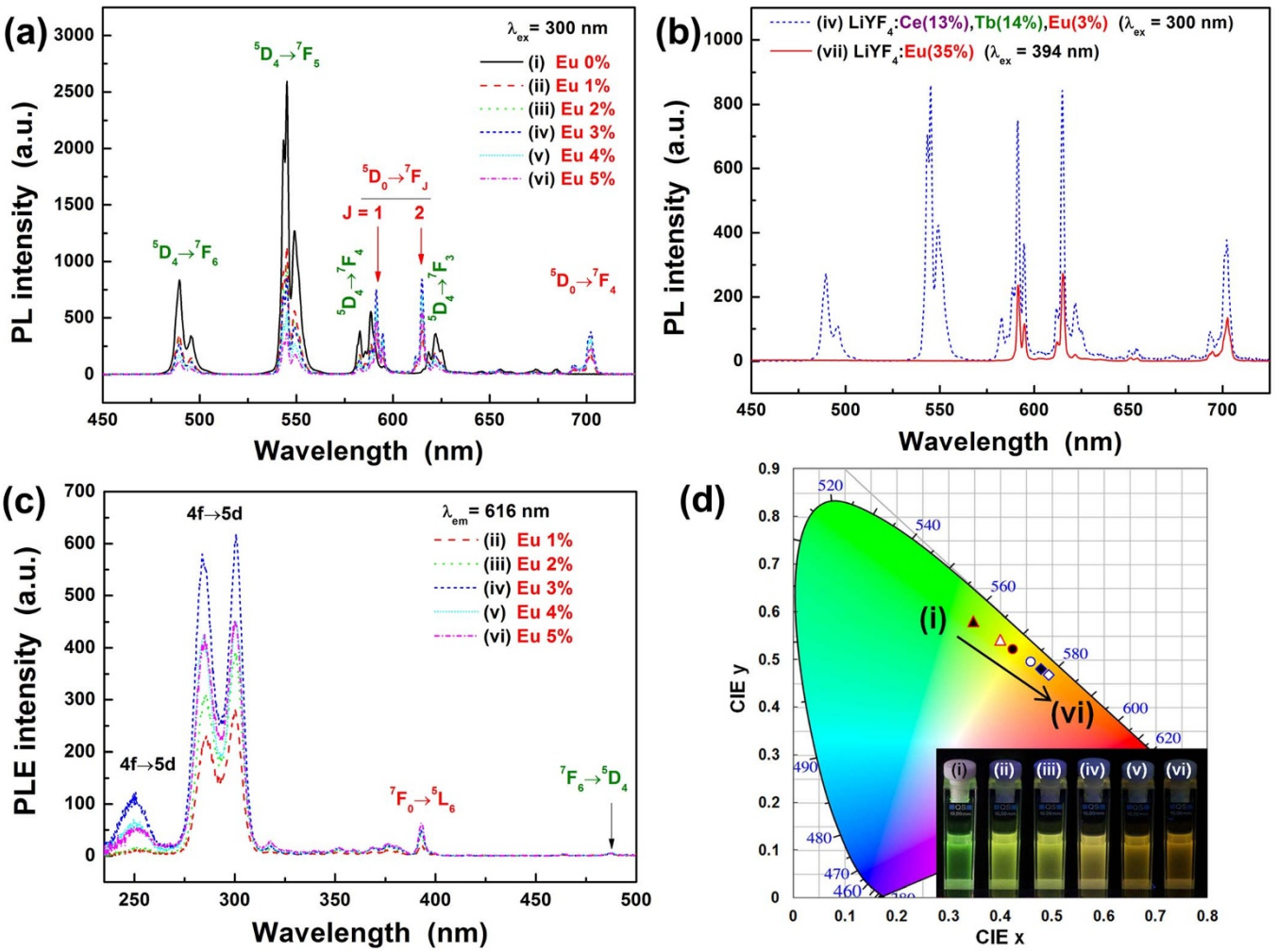

Figure 7 | (a), (b) PL and (c) PLE spectra, and (d) CIE color coordinates of $LiYF_4$:Ce(13%), Tb(14%), Eu(0–5%) [(i) 0%, (ii) 1%, (iii) 2%, (iv) 3%, (v) 4%, (vi) 5%, and (vii) $LiYF_4$:Eu(35%)]. Inset shows digital camera image of luminescent $LiYF_4$:Ce, Tb, Eu nanophosphor solution under hand held UV lamp.

fer from Tb^{3+} to Eu^{3+}, the energy transfer efficiency (η_{ET}) from the sensitizer Tb^{3+} ions to the activator Eu^{3+} ions was calculated by using the following equation[47]:

$$\eta_{ET} = 1 - \frac{I_S}{I_{S0}} \tag{3}$$

where I_S and I_{S0} are the emission intensities of the Tb^{3+} ions with and without Eu^{3+} ions, respectively. Figure 8b shows the calculated energy transfer efficiencies of the $Tb^{3+} \rightarrow Eu^{3+}$ pathway. As the Eu^{3+} concentration was increased from 1 to 5 mol%, the energy transfer efficiency correspondingly increased from 55.7 to 85.8%. A direct energy transfer from Ce^{3+} to Eu^{3+} was also confirmed by measuring the Ce^{3+} decay time (Figure S16). First, the Ce^{3+} decay of $LiYF_4$:Ce(15%) was compared with that of $LiYF_4$:Ce(15%), Eu(10%), which showed the strongest red emission from Eu^{3+} in the $LiYF_4$:Ce, Eu system, as shown in Figure S3. The Ce^{3+} decay time was shortened from 12.3 ns for $LiYF_4$:Ce(15%) to 0.6 ns for $LiYF_4$:Ce(15%), Eu(10%). This result indicates that energy was transferred from Ce^{3+} to Eu^{3+} even though the nanophosphors were not doped with Tb^{3+}. In addition, the Ce^{3+} decay time of $LiYF_4$:Ce(15%), Tb(15%), Eu(1%) was shorter than that of $LiYF_4$:Ce(15%), Tb(15%) (Figure S16(b)). Upon comparing the decay profile of the green-emitting $LiYF_4$:Ce(13%), Tb(14%) with that of the orange-emitting $LiYF_4$:Ce(13%), Tb(14%), Eu(5%), the Ce^{3+} decay time (0.4 ns) of the $LiYF_4$:Ce(13%), Tb(14%), Eu(5%) was found to be shorter than that (1.2 ns) of the $LiYF_4$:Ce(13%), Tb(14%), as shown in Figure S17. These results also support the pathway of $Ce^{3+} \rightarrow Eu^{3+}$ energy transfer. In summary, the energy transfer process in $LiYF_4$:Ce, Tb, Eu nanophosphors can be depicted as in Figure 8c. When the $LiYF_4$:Ce, Tb, Eu nanophosphors were excited with 300 nm UV light, the external UV light was absorbed by Ce^{3+} and then transferred to Tb^{3+}, followed by the transfer of this excited energy from Tb^{3+} to Eu^{3+}. Some of the excited energy was directly transferred from Ce^{3+} to Eu^{3+}. By considering the efficiencies of the $Ce^{3+} \rightarrow Eu^{3+}$ and $Ce^{3+} \rightarrow Tb^{3+} \rightarrow Eu^{3+}$ energy transfer pathways, we conclude that $Ce^{3+} \rightarrow Tb^{3+} \rightarrow Eu^{3+}$ energy transfer is more efficient than $Ce^{3+} \rightarrow Eu^{3+}$ energy transfer, based on the PL spectra shown in Figure S14. The stronger Eu^{3+} intensity of $LiYF_4$:Ce(13%), Tb(14%), Eu(1%) relative to that of $LiYF_4$:Ce(13%), Eu(1%) means that the $Ce^{3+} \rightarrow Tb^{3+} \rightarrow Eu^{3+}$ energy transfer pathway is more efficient than $Ce^{3+} \rightarrow Eu^{3+}$; in addition, Tb^{3+} acts as an efficient mediator for $Ce^{3+} \rightarrow Eu^{3+}$ energy transfer, which is consistent with previous reports[42,43]. As a consequence, the emission peaks are observed in the green and red spectral regions with intensity ratios that vary as a function of the Eu^{3+} concentration.

Nanophosphors with uniform size and shape can be dispersed in a polymer matrix[48]. To investigate the feasibility of applying $LiYF_4$:Ce, Tb, Eu nanophosphors to transparent display devices, the nanopho-

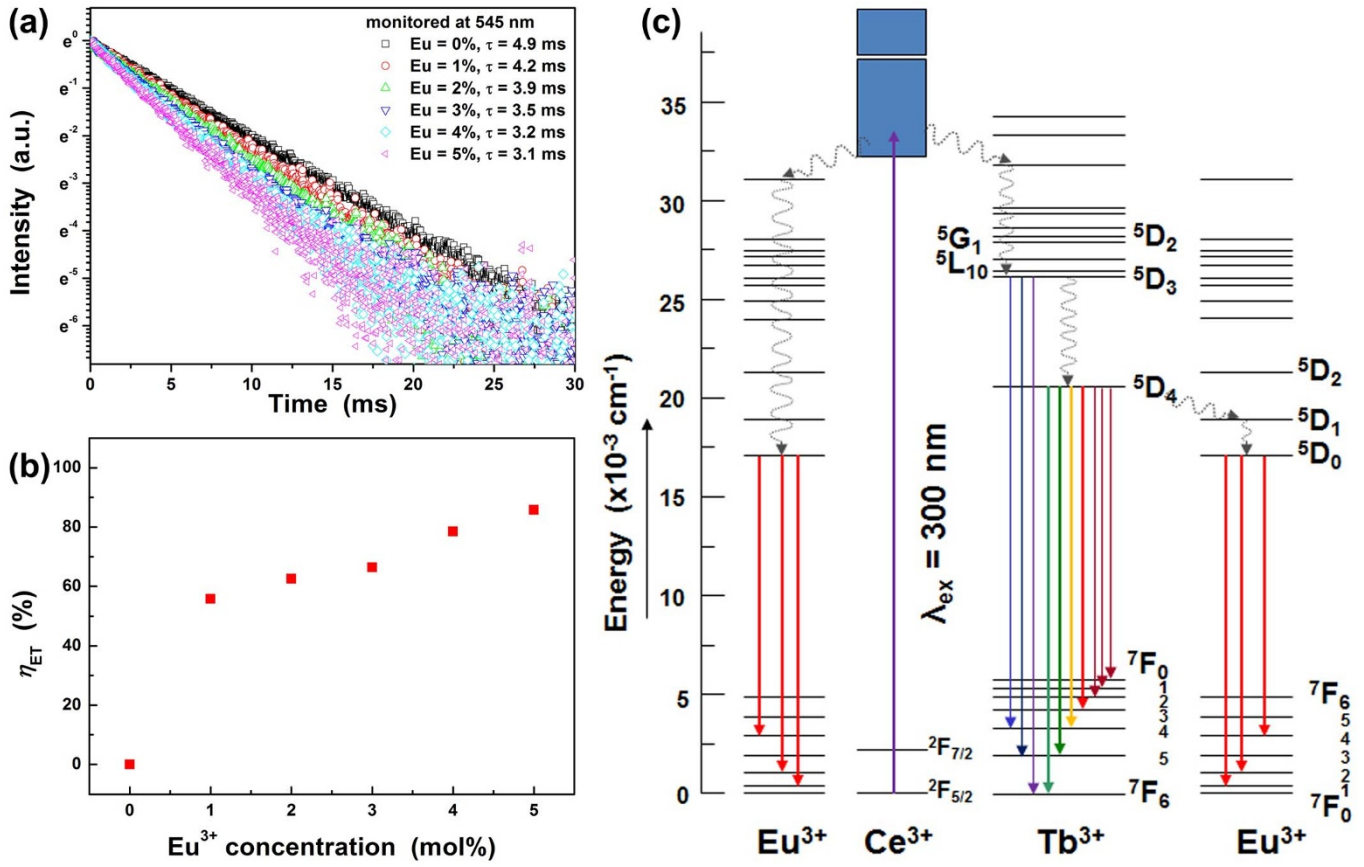

Figure 8 | (a) Decay profiles and (b) energy transfer efficiency for $Tb^{3+} \rightarrow Eu^{3+}$ energy transfer of $LiYF_4$:Ce(13%), Tb(14%), Eu nanophosphors with varying Eu^{3+} concentrations of 0, 1, 2, 3, 4, and 5%. (c) Schematic energy level diagram showing energy transfer.

sphors were incorporated into polydimethylsiloxane (PDMS) polymer. Figure 9 depicts photographs of the $LiYF_4$:Ce, Tb, Eu nanophosphor-PDMS composites taken under ambient indoor light and UV illumination. As shown in Figures 9a, S18a, and S19a, the $LiYF_4$:Ce, Tb, Eu nanophosphor-PDMS composites were highly transparent, and the background logos can clearly been seen. Transmittances of most nanophosphor-PDMS composites were higher than 75% in the visible spectral range (Figure S20). As we expected from the multicolor-emitting properties of the $LiYF_4$:Ce, Tb, Eu nanophosphors, the $LiYF_4$:Ce, Tb, Eu nanophosphor-PDMS composites also showed bright multicolor emission from green to orange, including yellow-green, greenish yellow, yellow, and orange yellow under illumination with a hand-held UV lamp (Figures 9b, S18b, and S19b). The emission of uniform visible light from the highly transparent nanophosphor-PDMS composites verifies that the $LiYF_4$:Ce, Tb, Eu nanophosphors were uniformly incorporated into the PDMS composites. The brightness of the nanophosphor-PDMS composites can be further enhanced by adapting the core/shell structured nanophosphors because the $LiYF_4$:Ce, Tb, Eu(1–5%)/$LiYF_4$ showed a stronger PL intensity than the $LiYF_4$:Ce, Tb, Eu(1–5%) core nanophosphors (Figure S21).

In summary, single-tetragonal-phase colloidal $LiYF_4$:Eu nanophosphors were successfully synthesized, and we investigated strategies to enhance Eu^{3+} emission from the $LiYF_4$:Eu-based nanophosphors. The luminescence properties of various nanophosphor architectures including $LiYF_4$:Eu/$LiYF_4$:Ce, Tb and $LiYF_4$:Ce, Tb/$LiYF_4$:Eu core/shell nanophosphors and $LiYF_4$:Ce, Tb, Eu nanophosphors were investigated. Among these structures, Ce^{3+}, Tb^{3+}, and Eu^{3+} triply-doped $LiYF_4$ nanophosphors exhibited strong Eu^{3+} emission via the efficient energy transfer of $Ce^{3+} \rightarrow Tb^{3+} \rightarrow Eu^{3+}$. In the case of $LiYF_4$:Eu nanophosphors, when sensitizers and activators were co-doped in the $LiYF_4$ NCs, the activator Eu^{3+} showed strong red emission. The Eu^{3+} emission was enhanced threefold via Ce and Tb sensitization. Owing to the $Ce^{3+} \rightarrow Tb^{3+}$ and $Ce^{3+} \rightarrow Tb^{3+} \rightarrow Eu^{3+}$ energy transfer pathways, green and red emission peaks were realized from the $LiYF_4$:Ce, Tb, Eu nanophosphors. In addition, the $LiYF_4$:Ce, Tb, Eu nanophosphors showed adjustable, bright multicolor emission from green to orange based on the Eu^{3+} concentration. These $LiYF_4$:Ce, Tb, Eu nanophosphors were uniformly incorporated into PDMS polymer, and the resulting nanophosphor-PDMS polymer composites also showed bright multicolor emission from green to orange, indicating that the $LiYF_4$:Ce, Tb, Eu nanophosphors have the potential for applications in transparent display devices.

Methods

Materials. $LiOH{\cdot}H_2O$ (99.995%), $YCl_3{\cdot}6H_2O$ (99.99%), $CeCl_3{\cdot}7H_2O$ (99.999%), $TbCl_3{\cdot}6H_2O$ (99.9%), $EuCl_3{\cdot}6H_2O$ (99.99%), NH_4F (99.99+%), oleic acid (OA, technical grade 90%), and 1-octadecene (ODE, technical grade 90%) were purchased from Aldrich and used without further purification. Sodium oleate (>97%) was obtained from TCI.

Synthesis of the $LiYF_4$:Eu nanophosphors. First, the lanthanide oleates [$Ln(oleate)_3$, Ln = Y and Eu] were prepared by adapting the synthesis reported by Hyeon and colleagues[49]. Then, 1 mmol of $Ln(oleate)_3$ complexes was loaded into a three-necked flask containing a solvent mixture of 10.5 mL OA and 10.5 mL ODE. The mixture was heated to 150°C for 40 min. After the reaction mixture cooled to 50°C, a methanol (MeOH) solution (10 mL) containing $LiOH{\cdot}H_2O$ (2.5 mmol) and NH_4F (4 mmol) was added to the reaction flask and stirred for 40 min. After removing the MeOH, the solution was heated to 320°C for 90 min under an Ar atmosphere. The as-synthesized nanophosphors were washed several times with ethanol and then dispersed in chloroform.

Synthesis of the $LiYF_4$:Eu/$LiYF_4$:Ce, Tb and $LiYF_4$:Ce, Tb/$LiYF_4$:Eu core/shell nanophosphors. For the synthesis of $LiYF_4$:Eu/$LiYF_4$:Ce, Tb nanophosphors, 0.7 mmol of $YCl_3{\cdot}6H_2O$, 0.15 mmol of $CeCl_3{\cdot}7H_2O$, and 0.15 mmol of $TbCl_3{\cdot}6H_2O$

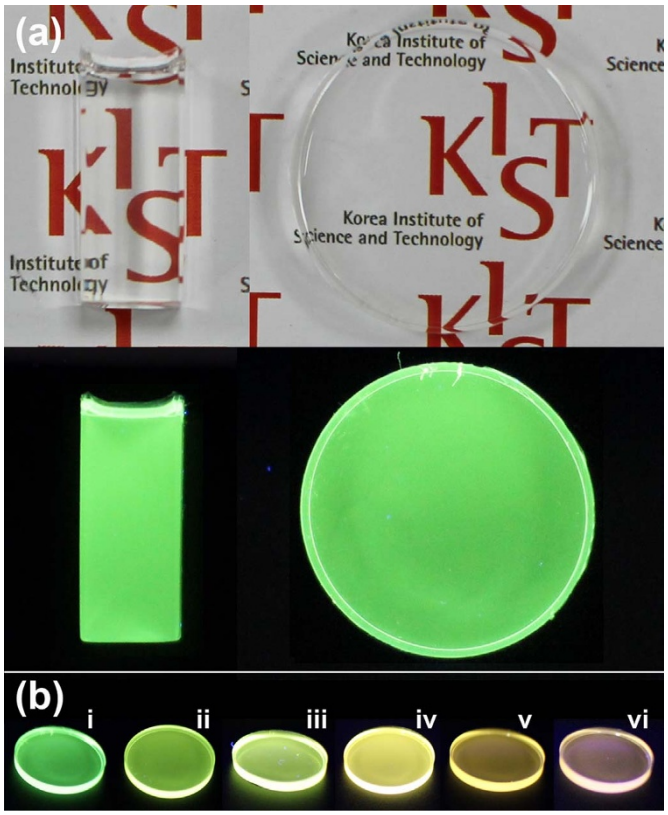

Figure 9 | Digital camera images of (a) $LiYF_4$:Ce (13%), Tb(14%), Eu(0%)-PDMS bar (left) and disk (right) under room light (upper panel) and UV lamp illumination (lower panel) and (b) $LiYF_4$:Ce, (13%), Tb(14%), Eu (0–5%)-PDMS disks under UV lamp illumination [i: 0%, ii: 1%, iii: 2%, iv: 3%, v: 4%, and vi: 5%]. The logo in (a) was reprinted with permission from Korea Institute of Science and Technology (KIST).

were loaded into a three-necked flask containing a solvent mixture of 10.5 mL OA and 10.5 mL ODE. The mixed solution was heated to 150°C for 40 min. After the solution was cooled to 80°C, 10 mL of $LiYF_4$:Eu chloroform solution was injected into the reaction flask. Then, the chloroform solvent was removed, and the reaction mixture was cooled to 50°C. A MeOH solution (10 mL) containing $LiOH{\cdot}H_2O$ (2.5 mmol) and NH_4F (4 mmol) was added to the reaction flask and then stirred for 40 min. After the MeOH was removed, the solution was heated to 300°C for 110 min under an Ar atmosphere. The as-synthesized nanophosphors were washed several times with ethanol and then dispersed in chloroform.

For the synthesis of $LiYF_4$:Ce, Tb/$LiYF_4$:Eu, $LiYF_4$:Ce, Tb core nanophosphors were prepared by using the same synthesis procedure as that for the synthesis of $LiYF_4$:Eu nanophosphors except the use of 1 mmol of $Ln(oleate)_3$ complexes [Ln = Y (70%), Ce (15%), and Tb (15%)]. Then, 0.65 mmol of $YCl_3{\cdot}6H_2O$ and 0.35 mmol of $EuCl_3{\cdot}6H_2O$ were loaded into a three-necked flask containing a solvent mixture of 10.5 mL OA and 10.5 mL ODE. The mixed solution was heated to 150°C for 40 min. After the solution was cooled to 80°C, 10 mL of $LiYF_4$:Ce, Tb chloroform solution was injected into the reaction flask. Then the chloroform solvent was removed, and the reaction mixture cooled to 50°C. A MeOH solution (10 mL) containing $LiOH{\cdot}H_2O$ (2.5 mmol) and NH_4F (4 mmol) was added to the reaction flask and stirred for 40 min. After the MeOH was removed, the solution was heated to 300°C for 110 min under an Ar atmosphere. The as-synthesized nanophosphors were washed several times with ethanol and then dispersed in chloroform.

Synthesis of the $LiYF_4$:Ce, Tb, Eu nanophosphors. As mentioned above, $Ln(oleate)_3$ complexes (Ln = Y, Ce, Tb, and Eu) were prepared and loaded into a three-necked flask. Other procedure was the same as that for the synthesis of the $LiYF_4$:Eu nanophosphors. For multicolor emission from the $LiYF_4$:Ce, Tb, Eu, the Eu^{3+} concentration was adjusted.

Synthesis of the $LiYF_4$:Ce, Tb, Eu/$LiYF_4$ nanophosphors. For the formation the $LiYF_4$ inorganic shell on the triply-doped $LiYF_4$:Ce, Tb, Eu core, 1 mmol of $YCl_3{\cdot}6H_2O$ was loaded into a three-necked flask containing a solvent mixture of 10.5 mL OA and 10.5 mL ODE. The mixed solution was heated to 150°C for 40 min. After the solution was cooled to 80°C and 10 mL of $LiYF_4$:Ce, Tb, Eu chloroform solution was injected into the reaction flask. Then, chloroform solvent was removed, and the reaction mixture cooled to 50°C. A MeOH solution (10 mL) containing $LiOH{\cdot}H_2O$ (2.5 mmol) and NH_4F (4 mmol) was added to the reaction flask and stirred for 40 min. After the MeOH was removed, the solution was heated to 300°C for 110 min under an Ar atmosphere. The as-synthesized core/shell nanophosphors were washed several times with ethanol and then dispersed in chloroform.

Preparation of the nanophosphor-PDMS composites. To prepare the multicolor-emitting $LiYF_4$:Ce, Tb, Eu-PDMS composites, 0.4 mL of the $LiYF_4$:Ce, Tb, Eu solution was thoroughly mixed with 10 mL of SYLGARD silicone elastomer 184 followed by the addition of a curing agent (1 mL). Finally, the nanophosphor-PDMS composites were aged overnight and then heat-treated at 80°C for 1 h.

Characterization. The crystal structures of the as-synthesized nanophosphors were determined using a Bruker D8 ADVANCE diffractometer with Cu K_α radiation (λ = 1.5406 Å) at 40 kV and 40 mA. The PLE and PL spectra and PL decay profiles of the nanophosphor solutions were obtained using a Hitachi F-7000 spectrophotometer. The size and morphology of the nanophosphors were investigated using a Tecnai G2 F20 (FEI Co.) operated at 200 kV. The EDS spectra were obtained using an EDAX EDS spectrometer PV9761.

1. Höppe, H. A. Recent Developments in the Field of Inorganic Phosphors. *Angew. Chem. Int. Ed.* **48**, 3572–3582 (2009).
2. Feldmann, C. *et al.* Inorganic Luminescent Materials: 100 Years of Research and Application. *Adv. Funct. Mater.* **13**, 511–516 (2003).
3. Blasse, G. & Grabmaier, B. C. *Luminescent Materials.* (Springer, Berlin, 1994).
4. van der Kolk, E. *et al.* Optimised co-activated willemite phosphors for application in plasma display panels. *J. Lumin.* **87–89**, 1246–1249 (2000).
5. Yadav, R. S. *et al.* Development of plasma display panel phosphors at National Physical Laboratory, New Delhi. *Indian J. Pure Appl. Phys.* **47**, 399–401 (2009).
6. Won, Y.-H. *et al.* Red-emitting $LiLa_2O_2BO_3:Sm^{3+}$, Eu^{3+} phosphor for near-ultraviolet light-emitting diodes-based solid-state lighting. *J. Electrochem. Soc.* **155**, J226–J229 (2008).
7. Wegh, R. T. *et al.* Visible quantum cutting in $LiGdF_4:Eu^{3+}$ through downconversion. *Science* **283**, 663–666 (1999).
8. Richards, B. S. Enhancing the performance of silicon solar cells via the application of passive luminescence conversion layers. *Sol. Energ Mater. Sol. Cells* **90**, 2329–2337 (2006).
9. van der Ende, B. M. *et al.* Near-Infrared Quantum Cutting for Photovoltaics. *Adv. Mater.* **21**, 3073–3077 (2009).
10. Rodríguez, V. D. *et al.* Towards broad range and highly efficient down-conversion of solar spectrum by Er^{3+}-Yb^{3+} co-doped nano-structured glass-ceramics. *Sol. Energy Mater. Sol. Cells* **94**, 1612–1617 (2010).
11. Yi, G. S. & Chow, G. M. Synthesis of Hexagonal-Phase $NaYF_4$:Yb,Er and $NaYF_4$:Yb,Tm Nanocrystals with Efficient Up-Conversion Fluorescence. *Adv. Funct. Mater.* **16**, 2324–2329 (2006).
12. Mai, H.-X. *et al.* High-Quality Sodium Rare-Earth Fluoride Nanocrystals: Controlled Synthesis and Optical Properties. *J. Am. Chem. Soc.* **128**, 6426–6436 (2006).
13. Wang, F. *et al.* Simultaneous phase and size control of upconversion nanocrystals through lanthanide doping. *Nature* **463**, 1061–1065 (2010).
14. Na, H. *et al.* Rational morphology control of β-$NaYF_4$:Yb,Er/Tm upconversion nanophosphors using a ligand, an additive, and lanthanide doping. *Nanoscale* **5**, 4242–4251 (2013).
15. Jang, H. S. *et al.* Bright dual-mode green emission from selective set of dopant ions in β-$Na(Y,Gd)F_4$:Yb,Er/β-$NaGdF_4$:Ce, Tb core/shell nanocrystals. *Opt. Express* **20**, 17107–17118 (2012).
16. Kim, S. Y. *et al.* Highly bright multicolor tunable ultrasmall β-$Na(Y,Gd)F_4$:Ce, Tb, Eu/β-$NaYF_4$ core/shell nanocrystals. *Nanoscale* **5**, 9255–9263 (2013).
17. Gai, S. *et al.* Recent Progress in Rare Earth Micro/Nanocrystals: Soft Chemical Synthesis, Luminescent Properties, and Biomedical Applications. *Chem. Rev.* **114**, 2343–2389 (2013).
18. Dai, Y. *et al.* In Vivo Multimodality Imaging and Cancer Therapy by Near-Infrared Light-Triggered trans-Platinum Pro-Drug-Conjugated Upconverison Nanoparticles. *J. Am. Chem. Soc.* **135**, 18920–18929 (2013).
19. Dai, Y. *et al.* Up-Conversion Cell Imaging and pH-Induced Thermally Controlled Drug Release from $NaYF_4:Yb^{3+}/Er^{3+}$@Hydrogel Core–Shell Hybrid Microspheres. *ACS Nano* **6**, 3327–3338 (2012).
20. Li, C. & Lin, J. Rare earth fluoride nano-/microcrystals: synthesis, surface modification and application. *J. Mater. Chem.* **20**, 6831–6847 (2010).
21. Wang, Z. L. *et al.* A Facile Synthesis and Photoluminescent Properties of Redispersible CeF_3, $CeF_3:Tb^{3+}$, and $CeF_3:Tb^{3+}/LaF_3$ (Core/Shell) Nanoparticles. *Chem. Mater.* **18**, 2030–2037 (2006).
22. Du, Y.-P. *et al.* Optically active uniform potassium and lithium rare earth fluoride nanocrystals derived from metal trifluroacetate precursors. *Dalton Trans.* **38**, 8574–8581 (2009).
23. Na, H. *et al.* Facile synthesis of intense green light emitting $LiGdF_4$:Yb,Er-based upconversion bipyramidal nanocrystals and their polymer composites. *Nanoscale* **6**, 7461–7468 (2014).
24. Chen, G. *et al.* Intense Visible and Near-Infrared Upconversion Photoluminescence in Colloidal $LiYF_4:Er^{3+}$ Nanocrystals under Excitation at 1490 nm. *ACS Nano* **5**, 4981–4986 (2011).

25. Mahalingam, V. *et al.* Colloidal Tm^{3+}/Yb^{3+}-Doped $LiYF_4$ Nanocrystals: Multiple Luminescence Spanning the UV to NIR Regions via Low-Energy Excitation. *Adv. Mater.* **21**, 4025–4028 (2009).
26. Wang, J. *et al.* Lanthanide-doped $LiYF_4$ nanoparticles: Synthesis and multicolor upconversion tuning. *C. R. Chim.* **13**, 731–736 (2010).
27. Boyer, J.-C. *et al.* Synthesis, characterization, and spectroscopy of $NaGdF_4$: Ce^{3+}, $Tb^{3+}/NaYF_4$ core/shell nanoparticles. *Chem. Mater.* **19**, 3358–3360 (2007).
28. Tu, D. T. *et al.* Time-Resolved FRET Biosensor Based on Amine-Functionalized Lanthanide-Doped $NaYF_4$ Nanocrystals. *Angew. Chem. Int. Ed.* **50**, 6306–6310 (2011).
29. Combes, C. M. *et al.* Optical and scintillation properties of Ce^{3+} doped $LiYF_4$ and $LiLuF_4$ crystals. *J. Lumin.* **71**, 65–70 (1997).
30. Kiliaan, H. S. *et al.* Energy transfer phenomena in Li(Y, Gd)F_4:Ce, Tb. *J. Lumin.* **35**, 155–161 (1986).
31. Zhang, X. *et al.* The synthesis and mechanism exploration of europium-doped $LiYF_4$ micro-octahedron phosphors with multilevel interiors. *Dalton Trans.* **43**, 5453–5461 (2014).
32. Wang, F. *et al.* Multicolor tuning of (Ln, P)-Doped YVO_4 nanoparticles by single-wavelength excitation. *Angew. Chem. Int. Ed.* **47**, 906–909 (2008).
33. Zhang, F. *et al.* Rare-Earth Upconverting Nanobarcodes for Multiplexed Biological Detection. *Small* **7**, 1972–1976 (2011).
34. DiMaio, J. R. *et al.* Controlling energy transfer between multiple dopants within a single nanoparticle. *Proc. Natl. Acad. Sci. U.S.A.* **105**, 1809–1813 (2008).
35. Wang, F. *et al.* Multicolour PEI/$NaGdF_4$:Ce^{3+}, Ln^{3+} nanocrystals by single-wavelength excitation. *Nanotechnology* **18**, 025701 (2007).
36. Ye, X. *et al.* Competition of shape and interaction patchiness for self-assembling nanoplates. *Nat. Chem.* **5**, 466–473 (2013).
37. Ptacek, P. *et al.* Crystal phase control of luminescing $NaGdF_4$:Eu^{3+} nanocrystals. *Adv. Funct. Mater.* **17**, 3843–3848 (2007).
38. Dorenbos, P. The 5d level positions of the trivalent lanthanides in inorganic compounds. *J. Lumin.* **91**, 155–176 (2000).
39. Kang, J. H. *et al.* Correlation of photoluminescence of (Y, Ln)VO_4:Eu^{3+} (Ln = Gd and La) phosphors with their crystal structures. *Solid State Commun.* **133**, 651–656 (2005).
40. Ghosh, P. *et al.* Energy transfer study between Ce^{3+} and Tb^{3+} ions in doped and core-shell sodium yttrium fluoride nanocrystals. *Nanoscale* **2**, 1196–1202 (2010).
41. Vetrone, F. *et al.* The Active-Core/Active-Shell Approach: A Strategy to Enhance the Upconversion Luminescence in Lanthanide-Doped Nanoparticles. *Adv. Funct. Mater.* **19**, 2924–2929 (2009).
42. Blasse, G. Energy Transfer from Ce^{3+} to Eu^{3+} in (Y,Gd)F_3. *Phys. Status Solidi A* **75**, K41–K43 (1983).
43. Zhang, X. *et al.* Tunable Luminescence and $Ce^{3+} \rightarrow Tb^{3+} \rightarrow Eu^{3+}$ Energy Transfer of Broadband-Excited and Narrow Line Red Emitting Y_2SiO_5:Ce^{3+}, Tb^{3+}, Eu^{3+} Phosphor. *J. Phys. Chem. C* **118**, 7591–7598 (2014).
44. Rack, P. D. *et al.* Determination of the Ce^{+3} bonding in the $Ca_{0.5}Sr_{0.5}Ga_2S_4$:Ce phosphor via x-ray photoelectron spectroscopy. *J. Appl. Phys.* **86**, 2377–2384 (1999).
45. Deng, S. *et al.* Mn–Ce oxide as a high-capacity adsorbent for fluoride removal from water. *J. Hazard. Mater.* **186**, 1360–1366 (2011).
46. Dexter, D. L. A Theory of Sensitized Luminescence in Solids. *J. Chem. Phys.* **21**, 836–850 (1953).
47. Cao, C. *et al.* Hydrothermal synthesis and enhanced photoluminescence of Tb^{3+} in Ce^{3+}/Tb^{3+} doped $KGdF_4$ nanocrystals. *J. Mater. Chem.* **21**, 10342–10347 (2011).
48. Chai, R. *et al.* In Situ Preparation and Luminescent Properties of CeF_3 and CeF_3:Tb^{3+} Nanoparticles and Transparent CeF_3:Tb^{3+}/PMMA Nanocomposites in the Visible Spectral Range. *J. Phys. Chem. C* **113**, 8070–8076 (2009).
49. Park, J. *et al.* Ultra-large-scale syntheses of monodisperse nanocrystals. *Nat. Mater.* **3**, 891–895 (2004).

Acknowledgments

This work was supported by the Dream project (2V03410) and Flagship project (2E24572) funded by the Korea Institute of Science and Technology (KIST), and the Pioneer Research Center Program through the National Research Foundation of Korea funded by the Ministry of Science, ICT & Future Planning (NRF-2013M3C1A3065040).

Author contributions

S.Y.K., Y.-H.W. and H.S.J. wrote the manuscript. H.S.J. designed the concept and the experiment method of the research. S.Y.K. carried out synthesis of materials, optical and structural characterization of the synthesized samples. Y.-H.W. analyzed experimental data. All authors reviewed manuscript.

Additional information

Supplementary information accompanies this paper at http://www.nature.com/scientificreports

Competing financial interests: The authors declare no competing financial interests.

How to cite this article: Kim, S.Y., Won, Y.-H. & Jang, H.S. A Strategy to enhance Eu^{3+} emission from $LiYF_4$:Eu nanophosphors and green-to-orange multicolor tunable, transparent nanophosphor-polymer composites. *Sci. Rep.* **5**, 7866; DOI:10.1038/srep07866 (2015).